Original Article
cnj.araku.ac.ir

Cite This: Colloid Nanosci. J. 3(1) (2025) 547-562 DOI: 10.61882/CNJ.3.1.547

Rheological Behaviors of Oil-Based Drilling Fluids in the Presence of Sawdust Charcoal Nanoparticles: A Molecular Dynamics Study

AmirMohammad Soltani[1], Mojtaba Rahimi[1,2]*

[1] Department of Petroleum Engineering, Kho.C., Islamic Azad University, Khomeinishahr, Iran
[2] Stone Research Center, Kho.C., Islamic Azad University, Khomeinishahr, Iran

ARTICLE INFO

Article History:
Received July 13, 2025
Revised September 22, 2025
Accepted September 24, 2025
Published September 27, 2025

Corresponding Authors:
Mojtaba Rahimi
Email:
mrahimi@iau.ac.ir

ABSTRACT

Drilling fluid performance is vital for operational efficiency, as it enhances the rate of penetration and ensures wellbore stability by preventing wellbore collapse. However, in harsh conditions (HPHT), the drilling efficiency and equipment longevity face significant threats. Specifically, the viscosity of drilling fluids decreases at high temperatures, exacerbating fluid loss. Mitigating fluid loss necessitates the deployment of temperature-stable additives, such as sawdust charcoal nanoparticles. These additives contribute to increased viscosity, fluid loss control, and improved filtration efficiency. The main objective of this study was to examine the rheological properties and filtration of bentonite, potassium chloride (KCl), and oil-based drilling fluids in the presence of sawdust charcoal nanoparticles using molecular dynamics (MD) simulations. First, the designed atomic samples were equilibrated, followed by an investigation into their structural evolution using the NVE ensemble. Throughout the MD simulation, to examine the rheological behavior of the target atomic structure, the changes in physical quantities, such as mean square displacement (MSD), shear stress, interaction energy, and viscosity, were analyzed. The main qualitative finding was that an increase in the initial temperature of the atomic sample enhanced atomic mobility within the simulation box; however, adding an additive to the initial structure reduced the sample's mobility due to an increase in attractive interatomic forces. Key quantitative findings included MSD increase to 2.39 Å, indicating enhanced atomic oscillation, and the absorption of 28 atoms into the porous material, suggesting improved fluid penetration. Shear stress reached 69.92 Pa, reflecting interatomic forces, while the interaction energy converged to -14.85 kcal/mol, highlighting its role in penetration thresholds. Overall, the study emphasized the need to balance fluidity and penetration efficiency to optimize drilling fluids for practical applications. The findings contributed to cost-effective and efficient drilling practices in the oil industry while addressing challenges in fluid behavior at the nanoscale.

KEYWORDS: *Bentonite, Potassium chloride, Drilling fluids, Sawdust charcoal nanoparticles, Rheological behaviors, Molecular dynamics simulation*

1-Introduction

Drilling fluids (DFs), sometimes called drilling mud (DM), are engineered liquids used in the oil and gas extraction process. They fulfill significant roles while drilling [1]. DF functions mainly to keep the drill bit lubricated and cool, and thus, reduces friction and heat during the drilling process [2]. Also, DFs help lift small bits of rock and soil from the hole and bring them to the surface for disposal [3]. DFs also maintain constant pressure (P) in the well to limit the premature entrance of oil, gas, or water. DFs also keep the well stable, where the wellbore does not deteriorate, and it remains strong [4]. DFs' ability to change shape and flow

is a critical factor that impacts many aspects of drilling. The driller, in a complex physical and chemical mechanical process in the drilling fluid, tries to maximize hole cleaning efficiency, the loss of P inside pipes and tubing, and the equivalent circulation density (ECD) while going down the well [5]. DF identifies major flow patterns within pipes and constricted areas, P variations, and tunes hydraulic setups to find optimum drilling [6]. The presence of effective fluid characteristics allows for the quick movement of drill cuttings away from the drill bit, which increases drilling efficiency, ensures drilling safety, and controls costs [7]. The proper characteristics of DF must be monitored to be able to give an accurate assessment of how well these DF characteristics perform. This is performed by monitoring flow characteristics, which will improve decision-making and efficiency in drilling operations [8]. Filtration effectiveness of DFs is a significant indicator of solid material movement ability, and the importance of flow is a factor in preventing clogging in bottom-hole equipment and surface facilities. Filtration is essential for wellbore stability, fluid loss reduction, and improved drilling operations efficiency [9]. The oil and gas sector routinely utilizes fluids that filter well while drilling in challenging conditions, including high-permeability areas, and predominantly during drilling in unstable shale conditions [10]. These characteristics are essential for good directional drilling. They play a significant role in the precision of filtration management; thus, proficiency decreases the likelihood of P differences, which could cause adverse effects on the rock formation, leading to well failure [11]. The use of bentonite (B) DM is beneficial because of the great suspension ability, thick viscosity (V), and fluid loss control and B DM forms an impermeable filter preventing fluid entry, while limiting formed damage, and is non-toxic and biodegradable making it useful in environmentally sensitive areas of operations [12, 13]. KCl DM, a water-based fluid with a long history in the drilling industry, is valued for its ability to control shale swelling, stabilize boreholes, inhibit formation damage, and minimize wellbore instability, making it suitable for sensitive environments, while also providing excellent filtration control and being non-toxic and environmentally friendly [14-16]. Oil-based mud offers superior lubrication and cooling, enhancing drilling efficiency and equipment longevity in challenging environments, while its high thermal stability, excellent fluid loss control, and formation stabilization reduce well collapse and formation damage [17, 18]. Coir fiber, derived from coconut husks, is gaining recognition as a sustainable additive in DM due to its high tensile strength, which enhances stability, and its fibrous structure that helps control fluid loss, while being biodegradable and environmentally friendly, thus minimizing toxicity and environmental impact [19, 20]. Pine sawdust, a byproduct of the wood industry, serves as an effective additive in DM by reducing fluid loss and maintaining well stability through its filter control properties and ability to form a protective filter cake [21]. Coal sawdust, or charcoal sawdust, is a promising additive in drilling mud formulations that offers various benefits and unique properties when incorporated into the mud [22].

From the past until now, extensive research consisting of experimental studies and numerical simulations has been carried out to clarify the complex interactions between DF components and geological formations, some of which are discussed below. Misbah et al. [16] studied the effects of temperature (T) on the stability of two viscosifier polymers, Flowzan (type A) and xanthan gum (type B), in water-based DM, and the finding showed that polymer A demonstrated superior performance in enhancing V, yield point, and gel strength, particularly at 250°F, while KCl addition improved thermal stability and maintained gel point recommendations for both polymers. Alimardanli et al. [23] found that replacing B in DFs with sawdust at optimal concentrations (0.0029% for particles <71 μm and 0.009% for 125-150 μm) led to a 7% reduction in fluid loss, with KCl fluids showing significant improvements when combined with sawdust. Oseh et al. [24] found that using 1 gr of sodium dodecyl sulfate with nano-hydroxyapatite in water-based DMs significantly improved thermal stability and V (increasing by 78.6% at 298 K and 79.2% at 353 K) while also reducing fluid loss by 31.8% at 298 K and 25% at 353 K. Khandaker et al. [25] found that adding SnO_2 nanoparticles to B water-based mud improved rheological and lubrication properties, with 0.1% by weight increasing plastic V and gel strength, and 0.5% reducing liquid loss and mud thickness by 8.1% and 34%, respectively, while 1% concentration achieved a maximum 14% reduction in the lubrication coefficient. Lalji et al. [26] found that biopolymer water-based DFs exhibited pseudo-

plastic properties, with filter volume increasing from 6.4 to 11.2 ml as ionic radius decreased, while potassium ions reduced filter loss, sodium caused salt crystal deposits, and magnesium enhanced long-term water preservation in shale samples. Abdullah et al. [27] found that adding 0.3 wt% polyethyleneimine-grafted graphene oxide to water-based DF at 160 °C significantly improved rheological properties, increasing the yield point/plastic V ratio and reducing filtration loss volume by 42% and 67%, respectively. Zhang et al. [28] studied the impact of petroleum-based components' atomic concentration on the atomic and rheological state of oil-based DFs using molecular dynamics (MD) simulations. They showed the challenges of utilizing water-based fluids that struggle to prevent shale enlargement and emphasized the development of eco-friendly and stable DFs with optimized rheological properties. The findings indicated that increasing the oil concentration from 15% to 30% enhances atomic mobility and permeability, thereby improving diffusion and reducing viscosity. The study also pointed out the significance of creating high-performance green drilling fluids to improve wellbore stability and reduce operational costs. Irfan and Busahmin [29] presented a study that attempted to improve the performance of DFs used in high-P high-T (HPHT) conditions to improve rheological behavior and shale inhibition potential. They studied the effect of single and dual-nanomaterial systems in base fluids to improve rheological behavior and shale inhibition ability. Five different nanomaterials (SiO_2, Al_2O_3, TiO_2, Fe_2O_3, and Fe_3O_4) were evaluated either on their own or in combinations with polymers. The rheological behavior of DFs was evaluated using the Herschel–Bulkley rheological model, with the main performance indicators being plastic V, fluid loss, and shale recovery. The results showed that while single-nanomaterial systems had small advantages, dual combinations significantly improved performance, suggesting synergistic effects among nanomaterials for use in advanced drilling fluids in extreme conditions.. ALBajalan et al. [30] demonstrated the improvement of nanocomposite DFs using synthesized TiO_2@Quillaja Saponin (QS)/Cr nanoparticles. The overall objectives was to enhance the rheological and filtration properties of DFs specifically for HPHT purposes. TiO_2@QS/Cr was synthesized and trialled as a function of concentration to show improvement in V and yield point, and to lower the fluid loss in filtration. These results indicated that the optimization of formulation would need to be considered so we avoid issues related to the agglomeration of nanoparticles at increased concentration, confirming the effectiveness of the nanocomposites in enhancing drilling fluid performance for HPHT conditions.

MD simulation is a fundamental computational method to assess the structure and function of biological macromolecules by allowing for the modeling of particle interactions as a function of time governed by physical laws. Because the systems of interest at the molecular level are complex, consisting of significant numbers of particles, it is typically impractical to evaluate systems of this complexity through analytical means. Therefore, MD is a critical method for permitting understanding of these systems. For instance, MD can be used to analyze the rheological specifications and filtration of DFs made with natural materials, such as nanoparticles of sawdust charcoal. By observing the molecular interactions of these particles with fluid components, researchers can evaluate how properties affect V, shear stress, and filtration, allowing formulations of DFs to be optimized for wellbore stability and to enhance more sustainable drilling efficiencies. To elaborate, our study of rheological specifications and filtration behavior of DFs, using sawdust charcoal nanoparticles as natural additives through the applied-MD simulations had two innovative aspects. The first aspect was that MD simulations provided an exact understanding of how the natural additives functioned within DF materials at the atomic and molecular scales. This understanding allowed an investigation to predict how the natural additives affected the overall fluid behaviours, such as viscosity, shear-thinning, and filtration behaviours. The second novel aspect of a natural sawdust charcoal nanoparticle as a natural additive was that it provided a sustainable approach to preparing DF systems. Natural materials will be renewable, biodegradable, and sustainable materials, as opposed to synthetic additives, and the DF industry is beginning to acknowledge the potential shift to sustainable materials to lower the industry's environmental footprint. Using natural sawdust charcoal nanoparticles in preparing DF formulations and evaluating the behaviour using MD simulations, researchers have new areas to develop excellent fluid systems that achieve performance requirements and maintain the

highest obligations to the environment.

In the present study, we examined the atomic and rheological behaviour of the sample. In this regard, we calculated and reported the following physical quantities: mean square displacement (MSD), amount of penetrating atoms, interaction energy (IE) (yield point), shear stress, and V. The work presented supported the optimisation of DFs for promoting further enhanced performance of these systems as better lubricant agents for drill bit activity, as well as more efficient drilling formations. The work also supported the development of more environmentally friendly and biodegradable fluids to help mitigate our environmental impact. The future results can lead to the development of new composite materials, increasing stability throughout changing conditions, and contributing to cost savings through opposed variances in materials sourced more locally. As a whole, the findings can support waste reduction and ultimately improve techniques for oil recovery in the oil and gas industry.

2-Simulation method

2-1- Simulation details

In the present study, the rheological properties and filtration of B, potassium chloride (KCl), and oil-based DFs in the presence of charcoal sawdust were investigated using MD simulation-based LAMMPS software. The basic atomic structures in the current research, which include the atomic/molecular compounds of B, potassium chloride, oil-based mud, and charcoal dross, are modeled using Avogadro software [31] and packed using PACKMOL software [32]. This prototype had 4588 atoms modeled in a cubic simulation box of 44×50×44 $Å^3$ (in X, Y, and Z directions, respectively), and periodic boundary conditions. Fig. 1 shows the initial atomic structure modeled. The structure modeled included a porous surface containing a quartz structure. This surface showed the rock or formation with which DF interacted. Quartz was a primary component of sandstone, a common reservoir rock type in oil and gas drilling operations.

Boundary conditions were considered periodically. To accurately represent the real structure of the DF system, it is necessary to use periodic boundary conditions in MD simulation. Periodic boundary conditions created an iterative, infinite system that mimics the larger-scale environment and enabled the simulation to capture the effects of the surrounding environment on the fluid components and their interactions. These boundary conditions effectively created an infinite, repeating system that mimicked the bulk environment of DFs. By doing so, the simulation avoids edge effects and artifacts that would otherwise arise in a finite system, allowing the model to capture interactions and behavior that were representative of macroscopic fluid properties. Table 1 presents the MD simulation settings adopted in this study. After modeling the studied structure, the equilibration in the modeling structure was checked. The equilibrium in the

Table 1. MD simulation settings in current computational research.

Computational Parameter	Parameter Ratio/Setting
MD Box Length	44×50×44 $Å^3$
Boundary condition	P P P
Number of Atoms	4588
Time Step	0.1 fs
Initial T	300 K
Damping T	10
Ensemble	NVE/NPT
Force field	Lennard-Jones/Coulomb
Equilibrium Time	10 ns
Total MD Time	20 ns

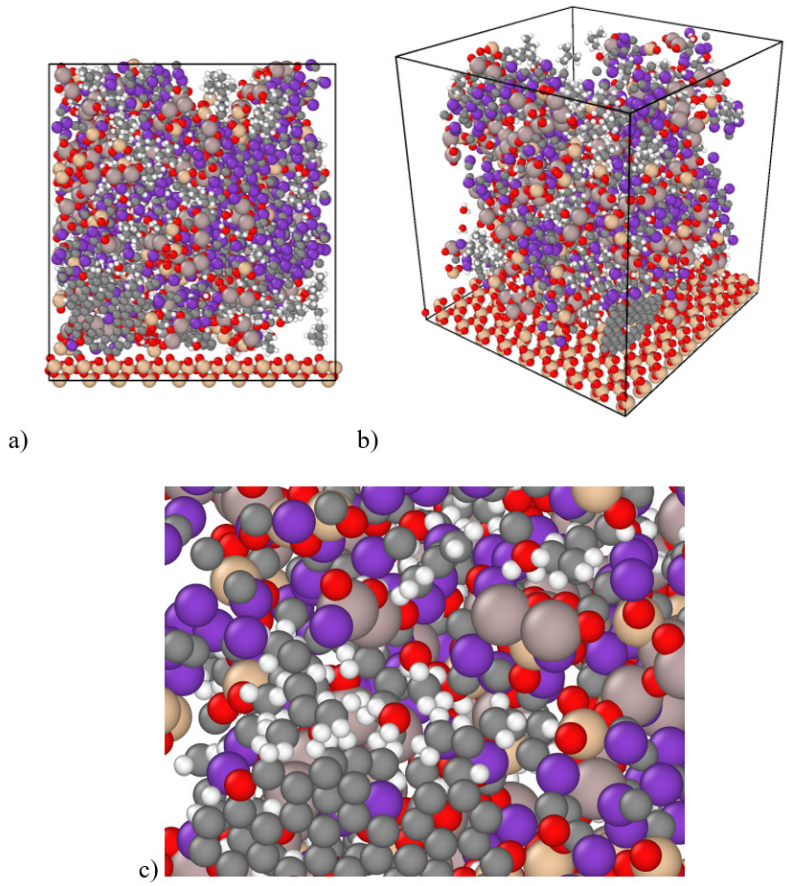

Fig. 1 The initial atomic structure modeled: a) front, b) perspective, and c) close-up view after the geometric optimization process in the present study.

simulated structures was expressed by investigating physical quantities, including the total T of simulated structures, the kinetic energy of simulated systems, the potential energy of simulated systems, and the total energy of simulated systems. At this stage, the NPT ensemble was used. T and P in the simulation were considered as ambient T and P using a Berenson barostat and Nose-Hoover thermostat. After ensuring the equilibration, the ensemble change of NVE and the rheological and atomic performance of the structure were calculated. Moreover, an external force, such as a P gradient and a body force, was applied to provide a more realistic representation of the filtration process.

2-2- The equilibration processes

After the modeling process, the thermodynamic behavior of the sample under the defined initial conditions (T= 300 K) was investigated. For this purpose, physical quantities, including T changes over time, were calculated and reported. From a numerical point of view, the value of T after 10 ns was 300.88 K. It was converged since this process occurred as a result of reducing the oscillation range of atoms, and finally, the structural stability of the target sample. The reduction in the oscillation range of atoms suggested that the particles within the fluid became more stable over time. In MD, atoms oscillate around their equilibrium positions, and a decrease in this oscillation indicates that the system is losing energy and reaching a more stable configuration. Fig. 2 exhibits T changes in the initial atomic sample under the initial conditions.

After the model was established, the system's thermodynamic behavior was examined at a T of 300 K. Properties, such as energy, P, and volume, were analyzed to understand the interactions and changes of materials over time. It was observed that the kinetic energy of the system reached a value of 45.67 kcal/mol after 10 ns, indicating stabilization as the particles moved less erratically and settled

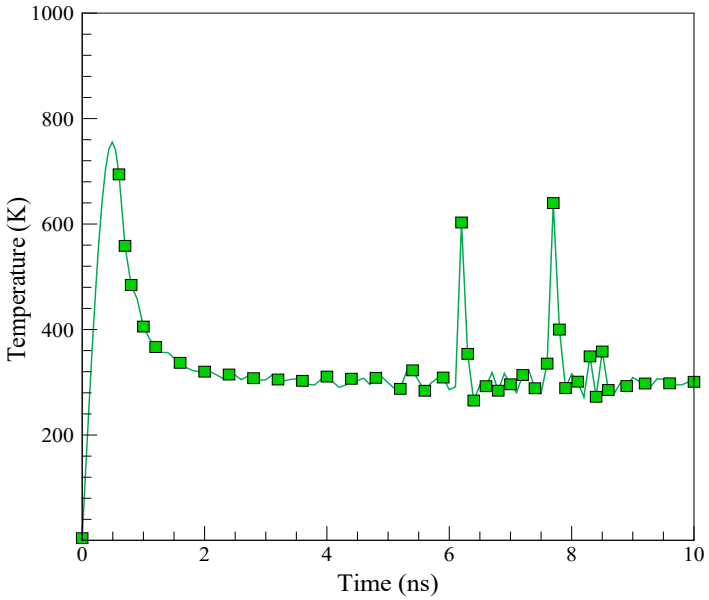

Fig 2. T changes in the initial atomic sample in the initial conditions

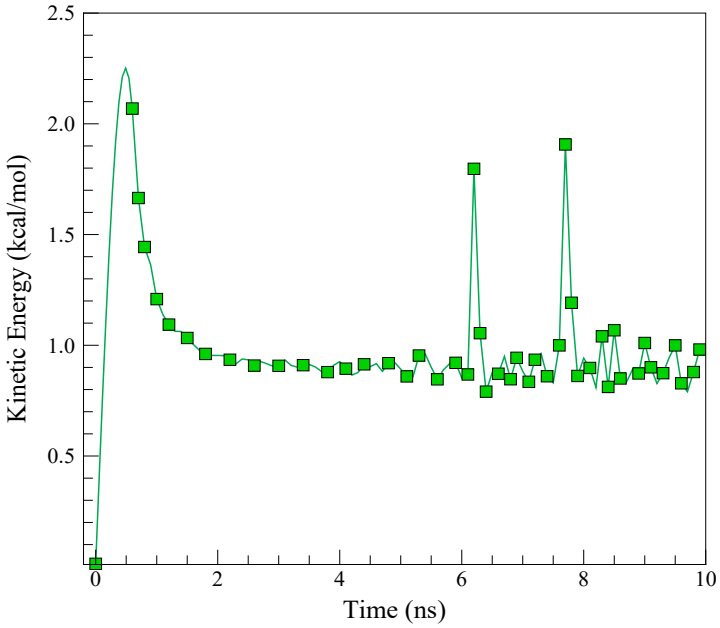

Fig 3. Kinetic energy changes in the initial atomic sample in the initial conditions

into a more stable configuration. The decrease in the oscillation range of atoms suggested that a more ordered and less chaotic state was being achieved, reflecting structural stability resulting from the interactions among the particles. Fig. 3 shows kinetic energy changes in the initial atomic sample under the initial conditions.

The potential energy outputs can be utilized to demonstrate the physical/structural stability of the modeled sample. This parameter is exhibited in Fig. 4. Numerically, the potential energy of the designed system had converged to 45.66 kcal/mol after 10 ns. This performance indicated the mean attraction force created among the variety of atoms inside the designed system. Thus, this performance was caused by the amplitude of atomic oscillations

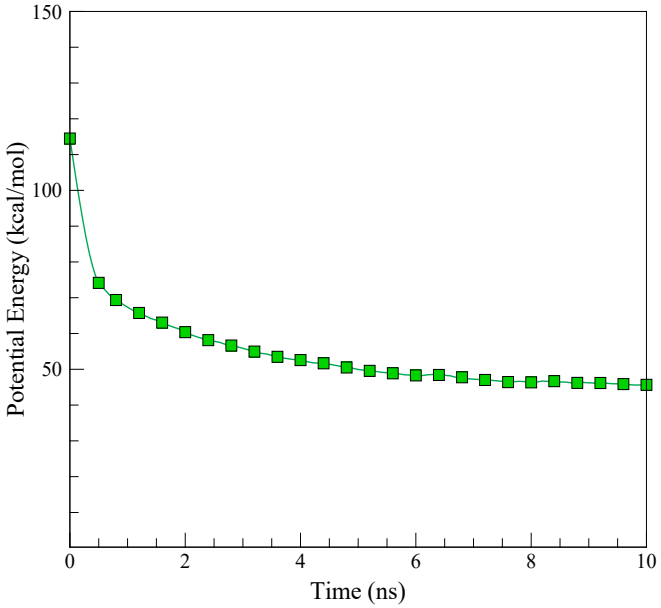

Fig. 4 Potential energy changes in the initial atomic sample in the initial conditions

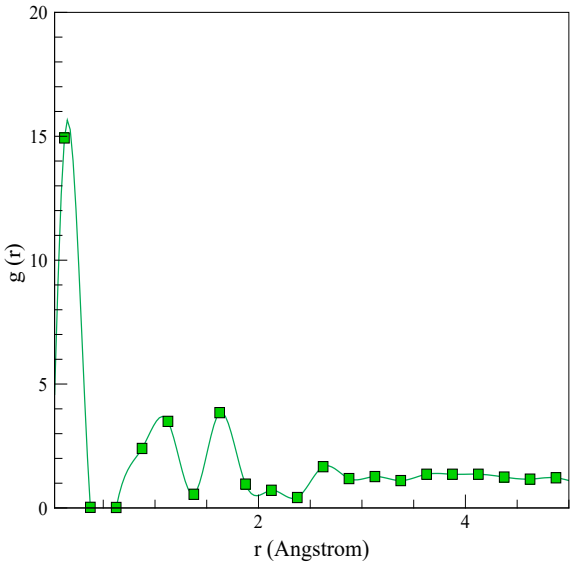

Fig 5. The RDF related to the atomic structure after equilibration of the atomic sample at 300 K

converging to a constant value according to their defined initial condition and structural unity expected in their actual applications._The radial distribution function (RDF), a key structural output in the analysis of an atomic sample, describes the relative arrangement of atoms in the system at a specified set of conditions. The peaks in the RDF indicated the average distances among atoms that result in the material's physical properties and organization (Fig. 5). In a more technical context, RDF was also used to confirm the simulation parameters used throughout the research. In a more practical sense, the results of simulations indicated that the atomic arrangements used in the simulations may be useful in real-world situations. As a result, the knowledge gained through collective simulations could help further advance the fields of materials science, nanotechnology, and chemical

engineering to allow for the design of new materials or help with the expanding breadth of applications for improved materials.

3- Results

In the current research, the atomic and rheological behaviors of the equilibrated sample were investigated for 10 ns. For this objective, the physical quantities, including MSD, the amount of penetration of the target structure into the porous material, the threshold IE between the target structure and the porous area, shear stress, and V, were calculated and reported.

The evolution of MSD is presented in Fig. 6. This quantity is one of the most important computational tools for measuring the random motion of a particle-rich sample, which was used in analyzing the evolution of atomic structures. The location of a particle in relation to a reference point, together with its deviation and spatial oscillations over time, are all represented by the mean square displacement in MD simulations. Consequently, MSD demonstrated how the intended atomic structure behaved. The particles started to migrate over time, which increased their displacement. Thermal and random energy factors caused the mean square displacement parameter to rise as the particles moved. According to the model results, the mean square displacement grew over time to 2.39 $Å^2$. This pattern showed that as time passed, the atoms' oscillation amplitude in the simulated sample increased.

Fig. 7 shows the number of atoms absorbed into the porous structure as a function of simulation time (ST), for the initial atomic sample with specified initial conditions. The results indicate that the number of absorbed atoms was 28 (after 10 ns). While the plot did not contain quantitative importance in the analysis of original data, it is significant for understanding the spatial and temporal nature of atomic motion and the interaction of atomic interactions in the porous material. As we observed the simulation unfold, the infiltration process allowed one to gain an overall sense of how it dissociated over time within the context of the original atomic sample and its interaction with the porous sample material. The results show that initially there was a rapid increase in the number of infiltrated atoms, indicating that the atoms were effectively infiltrating the porous structure. This behavior can be attributed to factors such as diffusion mechanisms and the availability of pathways in the porous matrix. As time passed, it was evident that the influx started to slow down, which would progress towards the probability of a saturation point approaching where the accessible

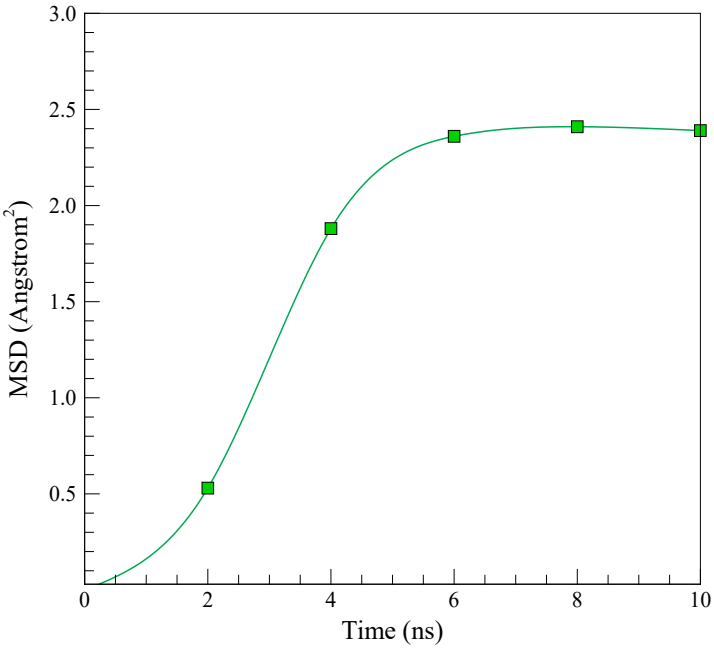

Fig 6. The changes of MSD according to ST in the initial atomic sample in the defined initial conditions

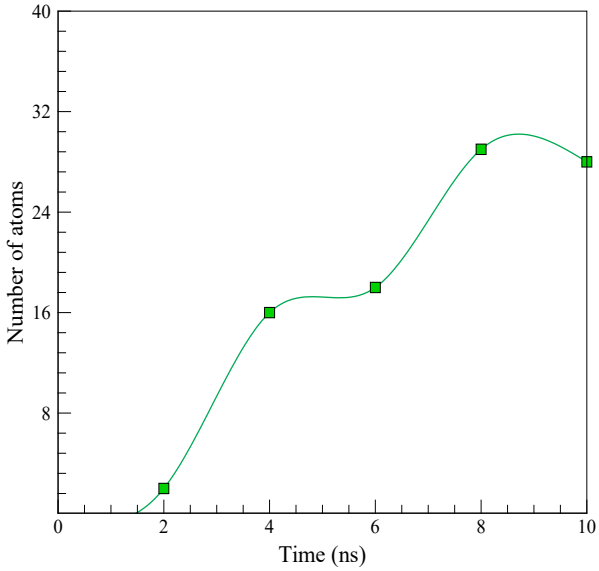

Fig 7. The number of atoms penetrating the porous structure is defined according to ST in the initial atomic sample under the initial conditions

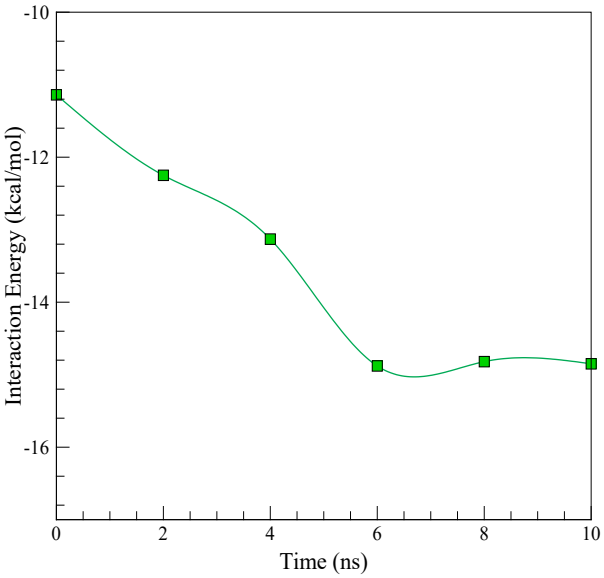

Fig 8. IE variations in terms of ST in the initial atomic sample in the defined initial conditions

sites in the porous material were occupied by sample atoms. Overall, these changes not only quantified atomic diffusion but also served as a valuable tool for analyzing and predicting material behavior at the atomic level, leading to improved design strategies for future studies involving porous structures.

In the continuation of this part, the changes in shear stress in the sample of the final structure were investigated. Considering the results presented in Fig. 8, as ST increased, the shear stress applied to the target atomic structure increased and reached 69.92 Pa. This process occurred as a result of the presence of interatomic forces in the structure and between the target and porous sample. On the other hand, to investigate the penetration threshold of the structure in the porous matrix, the IE between it and the porous sample will be of great importance. Previous studies reported that the shear stress of KCl-based DFs in the sample of the final structure

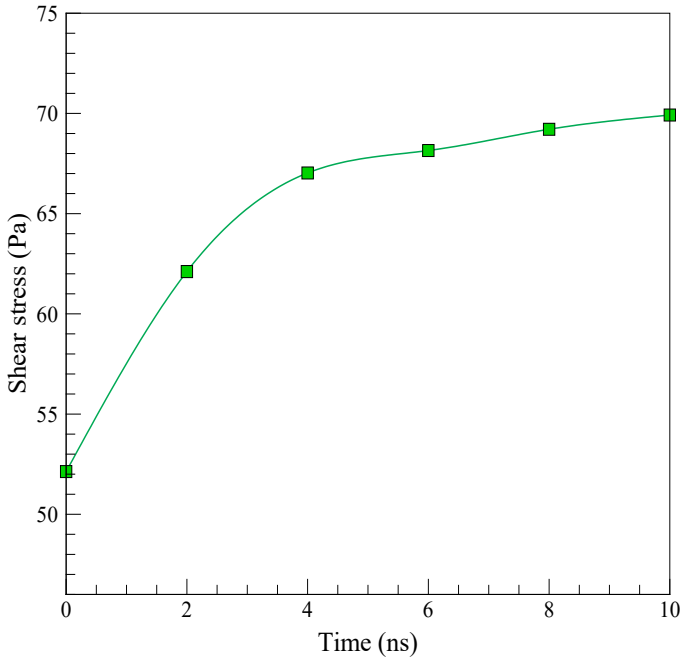

Fig 9. Shear stress changes according to ST in the initial atomic sample in the defined initial conditions

was in the range of 30-60 Pa [33-36].

Fig. 9 represents the change in IE during 10 ns. The results reveal that IE reached -14.85 kcal/mol. The results indicate that as the simulation progressed, DF not only became more effective at penetrating the porous material due to favorable IEs, but also showed increased resistance to flow as indicated by rising shear stress. This information is vital for optimizing DFs to ensure they perform well under operational conditions, balancing fluidity with effective penetration capabilities. These findings showed the relationship between shear stress and IE in DFs, providing insights into their behavior in porous media and the factors that affected their performance in practical applications.

Fig. 10 represents the change in the V during 10 ns. The results show V increased at 0.133 Pa.sec. Physically, this process was consistent with the narrowing of empty structural space by the increase in the fluctuations of atoms. It is important to note that even though V increased and the structural space narrowed for this process, there was no unstable structure in the atomic sample. Structurally stable atomic samples were important to recognize because even though the fluid was thicker and more difficult to efficiently flow, the stability of the atomic arrangement remained stable. In a previous study, Belayneh et al. [37] revealed that the apparent V of DFs increased with the addition of nanoparticles and was in approximately the same range as 100 cP (0.1 Pa.sec).

The study reported improved penetration, evidenced by the absorption of 28 atoms and a shear stress of 69.92 Pa, which were competitive with or slightly above the ranges observed for conventional additives like polymers or synthetic nanoparticles. Prior research documented shear stresses for KCl-based DFs in the final structure in the range of 30 to 60 Pa when using polymer-based additives [33-36]. Similarly, the V of 0.133 Pa·sec (133 cP) aligned with reported increases in V due to nanoparticle additions in B-based fluids, such as the study by Belayneh et al., where viscosities around 100 cP were observed with MoS_2 nanoparticles [37]. These values suggested that sawdust charcoal nanoparticles are capable of achieving rheological properties similar to or somewhat enhanced compared to conventional polymer or synthetic nanoparticle additives. In terms of cost-effectiveness, sawdust charcoal offered an environmentally friendly and potentially lower-cost alternative to synthetic nanoparticles, which often involved complex and costly manufacturing processes along with variability in quality [38, 39]. Additionally, bio-waste-derived additives like sawdust charcoal contributed to sustainability

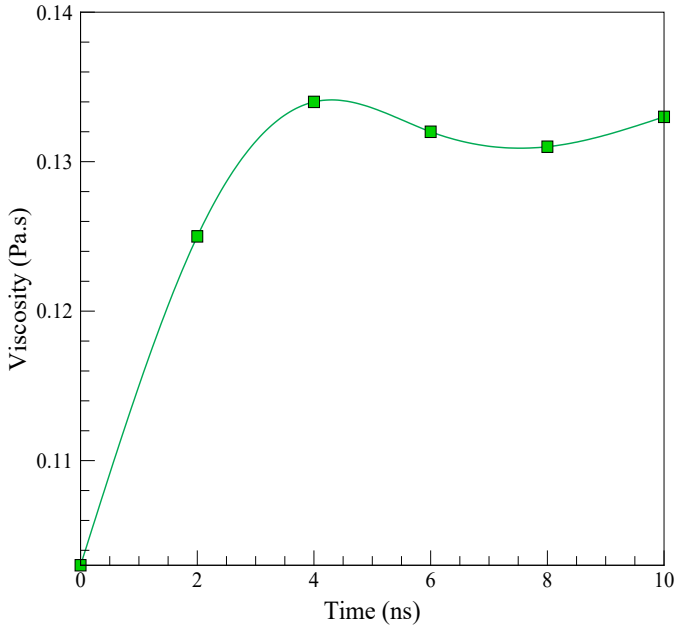

Fig 10. V variations of the target atomic structure based on ST in the initial atomic sample in the defined initial conditions

while maintaining effective rheological control. Regarding operational challenges linked to increased V, while higher V improved cuttings transport and fluid stability, it can indeed affect flow rates and pumping Ps. However, the reported V was within manageable limits and can be optimized through careful fluid formulation and real-time monitoring during drilling. Many studies showed that nanoparticle additives can increase V, but also enhance DF performance by reducing fluid loss and improving filter cake quality, leading to overall improved operational efficiency [40]. Thus, the sawdust charcoal nanoparticles balance enhanced performance metrics (such as improved penetration and shear stress) with operational feasibility and cost advantages, making them a promising additive for oil-based DFs. Based on the conclusions obtained from MD simulation and from an economic perspective, it can be said that using oil-based DFs augmented with sawdust charcoal nanoparticles is generally more cost-efficient than those with metallic nanoparticles in the heat transfer process. Sawdust charcoal, a bio-waste-derived material, was much cheaper and more sustainable in comparison to more expensive metallic nanoparticles like silicon oxide or iron oxides, as these bio-based nanoparticles provided sufficient enhancement in thermal conductivity while decreasing the total additive cost and environmental costs. The combination of a lower material cost and sufficient enhancement of DF properties (for example, V, filtration control, and thermal stability) made sawdust charcoal nanoparticles a cheaper option for enhancing heat transfer efficiencies in drilling operations than the typically more expensive metal-based nanoparticles. The greatest challenge in utilizing oil-based DFs with sawdust charcoal nanoparticles in heat transfer systems was keeping stable rheological and filtration properties under HPHT conditions, since the organic nature of sawdust charcoal may produce fluid behavior variability and degradation. A way around addressing the above challenge is likely to be in finding the optimization of concentration and formulations of nanoparticles for optimal dispersion and diminished agglomeration; thus, stabilizing V and filtration control. Furthermore, the conjunction of sawdust charcoal with other useful and compatible additives, which can include polymers or alternate nanocomposites, can help improve thermal stability and fluid performance.

4- Conclusion

The atomic and rheological behavior of DFs was investigated in this study. The structural evolution of samples was predicted using MD simulation-based LAMMPS software. First, the atomic samples

designed were balanced. The findings of this stage showed the convergence of T and kinetic energy at 300.88 K and 45.67 kcal/mol, respectively. The data obtained at this stage showed the decline of the atomic oscillation range over time inside the simulation box, as well as predicting the structural stability of the sample at the defined initial conditions. Then the structural evolution of samples was investigated using the NVE ensemble.

The most important results were as follows:

1) The MSD increased to 2.39 Å over time; 2) The process simulated resulted in 28 absorbed atoms in porous sample after 10 ns, suggesting higher penetration of DF over time; 3) The study showed how shear stress and V changed over time, indicating that shear stress reached 69.92 Pa and V increased to 0.133 Pa/sec; 4) After IE converged to -14.85 kcal/mol, the DF became more effective at penetrating porous medium while also exhibiting increased flow resistance. This emphasized the importance of balancing fluidity and penetration for optimizing DFs in practical applications.

Overall, the findings of this research can contribute to cost-effective and efficient drilling practices in the oil industry while addressing challenges in fluid behavior at the nanoscale.

Nomenclature

Acronym	Full Name
HPHT	High Pressure High Temperature
MD	molecular dynamics
MSD	mean square displacement
DFs	drilling fluids
DM	drilling mud
P	pressure
B	bentonite
V	viscosity
T	temperature
IE	interaction energy (yield point)

Original Research

This paper was written based on a Persian M.Sc. thesis completed by AmirMohammad Soltani.

Conflict of Interest

The authors declare there is no conflict of interest.

References

[1] J. P. Deville, Drilling fluids: Fluid Chemistry, Drilling and Completion, Elsevier, 2022. https://doi.org/10.1016/B978-0-12-822721-3.00010-1

[2] J. P. Simpson, Drilling fluids-today and tomorrow, J. Pet. Technol., 23(11) (1971) 1294-1298. https://doi.org/10.2118/3714-pa

[3] Guan, Z., Chen, T., Liao, H., Drilling fluids. In Theory and Technology of Drilling Engineering, Springer, Singapore, 2020. https://doi.org/10.1007/978-981-15-9327-7

[4] A. W. Ahmed, and E. Kalkan, Drilling fluids; types, formation choice and environmental impact, Int. J. Latest Technol. Eng. Manag. Appl. Sci, 8 (2019) 66-71. https://www.ijltemas.in/DigitalLibrary/Vol.8Issue12/66-71.pdf

[5] E. Hansen, Automatic evaluation of drilling fluid properties, University of Stavanger, Norway, 2012.

[6] C. Guria, R. Kumar, and P. Mishra, Rheological analysis of drilling fluid using Marsh Funnel, J. Pet. Sci. Eng., 105(2013) 62-69. https://doi.org/10.1016/j.petrol.2013.03.027 Actions

[7] N. Liu, D. Zhang, H. Gao, Y. Hu, and L. Duan, Real-time measurement of drilling fluid rheological properties: A review, Sensors, 21(11) (2021) 3592. https://doi.org/10.3390/s21113592

[8] A. Olatunde, M. Usman, O. Olafadehan, T. Adeosun, and O. Ufot, Improvement of rheological properties of drilling fluid using locally based materials, Pet. Coal., 54(1) (2012). https://www.vurup.sk/wp-content/uploads/dlm_uploads/2017/07/pc_1_2012_tunde_147_0.pdf

[9] A. E. Bayat, P. J. Moghanloo, A. Piroozian, and R. Rafati, Experimental investigation of rheological and filtration properties of water-based drilling fluids in presence of various nanoparticles, Colloids Surf. A: Physicochem. Eng. Asp., 555 (2018) 256-263. https://doi.org/10.1016/j.colsurfa.2018.07.001

[10] Z. Jeirani, and A. Mohebbi, Artificial neural networks approach for estimating filtration properties of drilling fluids, J. Jpn. Pet. Inst., 49(2) (2006) 65-70. https://doi.org/10.1627/jpi.49.65

[11] M. M. Barry, Y. Jung, J.-K. Lee, T. X. Phuoc, and M. K. Chyu, Fluid filtration and rheological properties of nanoparticle additive and intercalated clay hybrid bentonite drilling fluids, J. Pet. Sci. Eng., 127 (2015) 338-346. https://doi.org/10.1016/j.petrol.2015.01.012

[12] A.-M. Needaa, P. Pourafshary, A.-H. Hamoud, and A. Jamil, Controlling bentonite-based drilling mud properties using sepiolite nanoparticles, J. Pet. Explor. Dev., 43(4) (2016) 717-723.https://doi.org/10.1016/S1876-3804(16)30084-2

[13] K. Khan, S. A. Khan, M. U. Saleem, and M. Ashraf, Improvement of locally available raw bentonite for use as drilling mud, Open Constr. Build. Technol. J., 11(1) (2017). https://doi.org/10.2174/1874836801711010274

[14] D.-C. Huang, G. Xie, N.-Y. Peng, J.-G. Zou, Y. Xu, M.-Y. Deng, W.-C. Du, Y.-R. Xiao, J.-J. Huang, and P.-Y. Luo, Synergistic inhibition of polyethylene glycol and potassium chloride in water-based drilling fluids, J. Pet. Sci., 18 (2021) 827-838. https://doi.org/10.1007/s12182-020-00543-w

[15] M. Naeimavi, F. Khazali, M. Abdideh, and Z. Saadati, Potassium sorbate as substitute for KCl to shale inhibition in water-base drilling fluids, Energy Sources A: Recovery Util. Environ. Eff., 43(14) (2021)1691-1705. https://doi.org/10.1080/15567036.2019.1663303

[16] B. Misbah, A. Sedaghat, S. Balhasan, R. Elgaddafi, M. A. Malayer, R. N. Malhas, M. Omar, and M. Benomran, Enhancing thermal stability and filtration control for water-based drilling fluid using viscosifier polymers and potassium chloride additives, J. Geoenergy Sci. Eng., 230 (2023), 212235. https://doi.org/10.1016/j.geoen.2023.212235

[17] A. Patel, E. Stamatakis, S. Young, and J. Friedheim, Advances in inhibitive water-based drilling fluids-can they replace oil-based muds?, SPE, (2007) 106476-MS. https://doi.org/10.2118/106476-ms

[18] L. Jiancheng, Y. Peng, G. Jian, S. Yande, X. Kuang, and C. Shasha, A new type of whole oil-based drilling fluid, J. Pet. Explor. Dev., 41(4) (2014) 538-544. https://doi.org/10.1016/s1876-3804(14)60064-1

[19] R. Akbar, A. Hamid, and R. Sitaresmi, The Effect of Coconut Fibres, Banana Trunk Peel and Baggasse on the Lost Circulation of the Drilling Mud, J. Earth Energy Sci. Eng. Tech., 2(2) (2019). https://doi.org/10.25105/jeeset.v2i2.4674

[20] T. Salawudeen, A. O. Arinkoola, M. Jimoh, K. Salam, and E. O. Ogunmola, Effect of inert fibre on performance of B. eurycoma as rheology and filtration control additive in water-based drilling fluid, J. Pet. Eng., 2(3) (2016), 191-208. https://doi.org/10.1504/IJPE.2016.081763

[21] N. Ali, S. R. Manda, and R. H. Pulla, Pine Needles as Filter Loss Agent for Water-Based Mud, In International Conference on Materials for Energy Storage and Conservation, (2022) 131-138. https://doi.org/10.1007/978-981-99-2870-5_17

[22] E. Yalman, G. Federer-Kovacs, T. Depci, H. Al Khalaf, V. Aylikci, and M. G. Aydin, Development of novel inhibitive water-based drilling muds for oil and gas field applications, J. Pet. Sci. Eng., 210 (2022), 109907. https://doi.org/10.1016/j.petrol.2021.109907

[23] O. Alimardanli, "Effect of Saw dust on the Bentonite and KCL based drilling fluids: Experimental and Simulation studies," UIS University, Norway, 2023. https://uis.brage.unit.no/uis-xmlui/handle/11250/3091504

[24] J. O. Oseh et al., Rheological and filtration control performance of water-based drilling muds at different temperatures and salt contaminants using surfactant-assisted novel nanohydroxyapatite, J. Geoenergy Sci. Eng., 228 (2023) 211994. https://doi.org/10.1016/j.geoen.2023.211994

[25] A. A. B. Khandaker, N. Ahmed, and M. S. Alam, Rheology and lubricity characteristics study at different temperatures using synthesized SnO2 nanoparticles in KCl free bentonite water base mud, J. Pet. Res., 8(4) (2023) 541-549. https://doi.org/10.1016/j.ptlrs.2023.03.003

[26] S. M. Lalji, S. I. Ali, M. A. Khan, and R. Ghauri, Investigation of rheological behavior, filtration characteristics and microbial activity of biopolymer water-based drilling fluids containing monovalent and divalent cations, J. Chem. pap., 77(8) (2023) 4693-4704. https://doi.org/10.1007/s11696-023-02819-y

[27] A. H. Abdullah, S. Ridha, D. F. Mohshim, and M. A. Maoinser, "An experimental investigation into the rheological behavior and filtration loss properties of water-based drilling fluid enhanced with a polyethyleneimine-grafted graphene oxide nanocomposite," J. RSC Adv., 14(15) (2024) 10431. https://doi.org/10.1039/D3RA07874D

[28] X. Zhang, H. Yu, R. Sabetvand, and A. Brahmia, Effect of the atomic concentration of petroleum base components on the atomic and rheological behavior of the structure of bentonite, potassium chloride, and oil-base drilling fluids using molecular dynamics simulation, J. ICHMT, 166 (2025) 109146. https://doi.org/10.1016/j.icheatmasstransfer.2025.109146

[29] M. W. Bin Irfan, and B. Busahmin, Rheological Characterization and Shale Inhibition Potential of Single-and Dual-Nanomaterial-Based Drilling Fluids for High-Pressure High-Temperature Wells, Processes, (13)(7) (2025), 1957. https://doi.org/10.3390/pr13071957

[30] A. R. ALBajalan, A. A. Rasol, H. F. M. Ameen, P. T. Jaf, and A. Abumalek, Enhanced performance of nanocomposite drilling fluids with synthesized TiO2 Quillaja saponin Cr nanoparticles and their impact on rheology and filtration, J. Sci. Rep., 15(1) (2025) 27667. https://doi.org/10.1038/s41598-025-13459-5

[31] M. D. Hanwell, D. E. Curtis, D. C. Lonie, T. Vandermeersch, E. Zurek, and G. R. Hutchison, Avogadro: an advanced semantic chemical editor, visualization, and analysis platform, cheminformatics, 4(1) (2012) 17. https://doi.org/10.1186/1758-2946-4-17

[32] L. Martínez, R. Andrade, E. G. Birgin, and J. M. Martínez, PACKMOL: A package for building initial configurations for molecular dynamics simulations, J. Comput. Chem., 30(13) (2009) 2157-2164. https://doi.org/10.1002/jcc.21224

[33] G. Wang, and H. Du, Rheological properties of KCl/Polymer type drilling fluids containing particulate loss prevention material, j. Appl. Rheol., 28(3) (2018) 201835727. DOI:10.3933/ApplRheol-28-35727

[34] C. B. Bavoh, T. N. Ofei, B. Lal, A. M. Sharif, M. H. B. Shahpin, and J. D. Sundramoorthy, Assessing the impact of an ionic liquid on NaCl/KCl/polymer water-based mud (WBM) for drilling gas hydrate-bearing sediments, J. Mol. Liq., 294 (2019) 111643. https://doi.org/10.1016/j.molliq.2019.111643

[35] M. Edalatfar, F. Yazdani, and M. B. Salehi, Synthesis and identification of ZnTiO3 nanoparticles as a rheology modifier additive in water-based drilling mud, J. Pet. Sci. Eng., 201 (2021) 108415. https://doi.org/10.1016/j.petrol.2021.108415

[36] M. Du, P. Liu, P. L. Clode, J. Liu, B. Haq, and Y.-K. Leong, Impact of additives with opposing effects on the rheological properties of bentonite drilling mud: Flow, ageing, microstructure and preparation method, J. Pet. Sci. Eng., (192) (2020) 107282. https://doi.org/10.1016/j.petrol.2020.107282

[37] M. Belayneh, B. Aadnøy, and S. M. Strømø, MoS2 nanoparticle effects on 80° C thermally stable water-based drilling fluid, Materials, 14(23) (2021) 7195. https://doi.org/10.3390/ma14237195

[38] A. N. Okon, J. U. Akpabio, and K. W. Tugwell, Evaluating the locally sourced materials as fluid loss control additives in water-based drilling fluid, Heliyon, 6(5) (2020). https://doi.org/10.1016/j.heliyon.2020.e04091

[39] R. Rafati, S. R. Smith, A. S. Haddad, R. Novara, and H. Hamidi, Effect of nanoparticles on the modifications of drilling fluids properties: A review of recent advances, J. Pet. Sci. Eng., 161 (2018) 61-76. https://doi.org/10.1016/j.petrol.2017.11.067

[40] R. Ikram, B. Mohamed Jan, A. Sidek, and G. Kenanakis, "Utilization of eco-friendly waste generated nanomaterials in water-based drilling fluids; state of the art review," Materials, 14(15) (2021) 4171. https://doi.org/10.3390/ma14154171

[41] D. Rapaport, Molecular dynamics simulation, J. Comput. Sci. Eng., 1(1) (2002) 70-71. https://doi.org/10.1109/5992.743625

[42] L. Verlet, Computer experiments on classical fluids. I. Thermodynamical properties of Lennard-Jones molecules, J. Phys. Rev., 159(1) (1967) 98. DOI: https://doi.org/10.1103/PhysRev.159.98

[43] W. Press, S. Teukolsky, W. Vetterling, and B. Flannery, Second-order conservative equations, Numerical recipes: The art of scientific computing, 3rd ed., Cambridge University Press, New York, 2007.

[44] J. E. Lennard-Jones, Cohesion, Proceedings of the Physical Society, 43(5) (1931) 461. https://doi.org/10.1088/0959-5309/43/5/301

[45] H. J. Berendsen, J.-R. Grigera, and T. P. Straatsma, The missing term in effective pair potentials, J. Phys. Chem.,

91(24) (1987) 6269-6271. https://doi.org/10.1021/j100308a038

[46] A. K. Rappé, C. J. Casewit, K. Colwell, W. A. Goddard III, and W. M. Skiff, UFF, a full periodic table force field for molecular mechanics and molecular dynamics simulations, J. Am. Chem. Soc., 114(25) (1992) 10024-10035. https://doi.org/10.1021/ja00051a040

[47] Lammps manual, harmonic bond style, https://docs.lammps.org/bond_harmonic.html, 2003-2025.

[48] Lammps manual, harmonic angle style, https://docs.lammps.org/angle_harmonic.html, 2003-2025.

Appendix

A. MD Simulation

Newton's laws of motion form the foundation for how MD simulation operates. Using these laws to analyze the minuscule particles within a system allows us to replicate the dynamics of their movement over time. This approach allows us to determine the force acting on a particle referred to as "i" through the potential function outlined in Eq. (a-1) [41].

$$F_i = -\nabla_i U \qquad \text{(a-1)}$$

Essentially, Newton's concepts about motion explain that the movement of a spherical particle, like a molecule or a small item, occurs because of an external force, known as F_i. Newton's second law illustrates the relationship between the applied force and the resulting motion. Eq. (a-2) [41] provides an explanation for this.

$$F_i = m_i a_i \qquad \text{(a-2)}$$

m (mass unit) is the mass of a single particle, which is considered to be constant regardless of position, velocity, or time. Additionally, acceleration can be derived from the following relationship [41]:

$$a_i = \frac{d^2 r_i}{dt^2} \qquad \text{(a-3)}$$

Here, r_i is a distance vector indicating the particle's position relative to a fixed reference frame, and by integrating the above relationships, one can derive a relationship that expresses the particles' positions through the potential function [41]:

$$-\frac{dU}{dr_i} = m_i \frac{d^2 r_i}{dt^2} \qquad \text{(a-4)}$$

The Velocity Algorithm is a highly accurate and efficient method for numerically integrating Newton's equations of motion, widely used in various simulations, including sustainable energy problems. This algorithm provides stable and precise solutions, making it a preferred choice for researchers to calculate the dynamic paths of particles in simulated systems. In MD simulations, particle displacements and velocities are computed by incorporating statistical mechanics to analyze the characteristics of the studied systems. The algorithm is detailed in Eq. a-5 [42, 43].

$$r_i(\mathrm{t} + \Delta\mathrm{t}) = 2\, r_i(t) - r_i(t - \Delta t) + \left(\frac{d^2 r_i}{dt^2}\right)(\Delta t)^2 \qquad \text{(a-5)}$$

In MD simulations, defining the potential function and interparticle forces is crucial for obtaining reliable results. The force field is essential for modeling interatomic interactions and calculating the potential energy of the particle system. Accurately selecting the force field enhances the simulation's ability to predict and replicate the actual physical processes. Potential functions are typically categorized into bonded and non-bonded interactions, and the total potential energy of a system is determined by summing these interactions [41].

$$E_{total} = E_{bonded} + E_{nonbonded} \qquad \text{(a-6)}$$

Non-bonded potentials involve various types of interaction potential energy, which will be derived from the combined Lennard-Jones, Vashishta, and Coulombic force potential functions in future work. The Lennard-Jones potential, a fundamental mathematical model, approximates the interactions between neutral particles or molecules and is commonly expressed in a specific equation format [44].

$$U_{LJ} = 4\varepsilon_{ij}\left[\left(\frac{\sigma_{ij}}{r_{ij}}\right)^{12} - \left(\frac{\sigma_{ij}}{r_{ij}}\right)^{6}\right] \qquad r < r_c \qquad \text{(a-7)}$$

In Eq. (a-7), ε_{ij} (energy unit) represents the depth of the potential well, representing the strength of the attractive interaction among particles, σ_{ij} (length unit) is the finite distance where the potential function becomes zero, indicating the size of particles in the system, and r_{ij} denotes the cut-off radius, typically averaging 12 Å in

simulations. Interatomic interactions are vital in MD, as refining their expressions enhances the accuracy of predictions. However, this increased precision can reduce computational velocity and prolong simulation times. Additionally, the cut-off radius varied based on specific applications of MD in different systems and the physical concepts being studied. Also, the values of r and each of the interactions among the particles present in the simulation box were calculated using Eqs. (8-9) [45]:

$$\varepsilon_{ij} = \sqrt{\varepsilon_i \varepsilon_j} \qquad \text{(a-8)}$$

$$\sigma_{ij} = \frac{\sigma_i + \sigma_j}{2} \qquad \text{(a-9)}$$

The σ_{ij} and ε_{ij} for the present particles are given in Table a-1.

The harmonic potential serves as a widely utilized mathematical framework in MD simulations, particularly in LAMMPS, to effectively model covalent bond interactions among atoms. It is based on the premise that the force acting on atoms is proportional to the displacement of the bond length from its equilibrium position. Essentially, the potential energy associated with a bond varies quadratically with the extent of deviation from its optimal length. This method is crucial for accurately capturing the mechanical behavior of materials at the atomic scale, enabling bonds to undergo both elongation and compression. The potential energy is expressed by the following formula [47]:

$$V_{bond} = \frac{1}{2} k(r - r_0)^2 \qquad \text{(a-10)}$$

V_{bond} represents the potential energy of the bond depending on the interatomic distance, r, with r_0 denoting the bond's equilibrium length. The parameter k indicates the bond stiffness, which quantifies the resistance of the bond to changes in length. This quadratic relationship effectively modeled covalent bond behavior by illustrating that bond energy increases proportionally to how far the bond length deviates from its equilibrium state.

Table a-1. Lennard-Jones potential function parameters for the present particles [45, 46].

Particle type	ε (kcal/mol)	σ (Å)
C	0.105	3.851
Si	0.402	4.295
O	0.06	3.5
Al	0.505	4.499
H	0.274	4.035
K	0.035	3.812
Cl	0.2278	3.947

Table a-2. Typical equilibrium bond lengths for various bond types.

Bond Type	Bonds (Å)	Bond Type	Bonds (Å)
Al-Cl	2.034	Cl-K	2.94
Al-K	2.99	Cl-O	1.647
Al-O	1.697	Cl-Si	1.924
Al-Si	1.974	H-O	0.98
C-C	1.53	K-K	3.896
C-Cl	1.757	K-Si	2.88
C-H	1.09	O-Si	1.587
C-O	1.42	Si-Si	1.864
Cl-Cl	1.984		

Table a-3 The equilibrium angles in angular bond interaction.

Angles	Angles (θ)	Angles	Angles (θ)	Angles	Angles (θ)
Al-Cl-Al	180	C-O-H	104.51	H-C-O	109.471
Al-Cl-Cl	180	Cl-Al-Cl	109.471	H-O-H	104.51
Al-Cl-K	180	Cl-Al-K	109.471	K-Al-K	109.471
Al-Cl-O	180	Cl-Al-O	109.471	K-Al-O	109.471
Al-Cl-Si	180	Cl-Al-Si	109.471	K-Al-Si	109.471
Al-K-Al	180	Cl-C-H	109.471	K-Cl-K	180
Al-K-Cl	180	Cl-Cl-Cl	180	K-Cl-O	180
Al-O-Al	104.51	Cl-Cl-K	180	K-Cl-Si	180
Al-O-Cl	104.51	Cl-Cl-O	180	K-K-K	180
Al-O-H	104.51	Cl-Cl-Si	180	K-K-Si	180
Al-O-Si	104.51	Cl-K-Cl	180	K-Si-K	109.471
Al-Si-Cl	109.471	Cl-K-K	180	K-Si-O	109.471
Al-Si-K	109.471	Cl-K-Si	180	O-Al-O	109.471
Al-Si-O	109.471	Cl-O-Cl	104.51	O-Al-Si	109.471
C-C-C	109.471	Cl-O-H	104.51	O-C-O	109.471
C-C-Cl	109.471	Cl-O-Si	104.51	O-Cl-O	180
C-C-H	109.471	Cl-Si-Cl	109.471	O-Cl-Si	180
C-C-O	109.471	Cl-Si-K	109.471	O-Si-O	109.471
C-Cl-C	180	Cl-Si-O	109.471	O-Si-Si	109.471
C-O-C	104.51	H-C-H	109.471	Si-O-Si	104.51

Harmonic potentials were often used within LAMMPS to describe the angles that were formed by three atoms, more accurately representing the molecular geometry. Angular potentials quantify the energy cost or penalty for a bond angle to deviate from its most preferred value. Generally speaking, the angular harmonic potential is in the form of a quadratic function, suggesting that energy increases as the angular distance moves away from the ideal position. This allows for realistic modeling of molecular conformation by placing angular constraints, while molecules can appropriately react to different environmental effects and forces. The angular potential can be expressed by the following equation [48]:

$$V_{angle} = \frac{1}{2} k_\theta (\theta - \theta_0)^2 \qquad \text{(a-11)}$$

V_{angle} denotes the potential energy linked to the angle θ formed by three bonded atoms, where θ_0 represents the equilibrium angle and k is the force constant that reflects the angle's stiffness. The quadratic nature ensured that any variation from θ_0 leads to a rise in potential energy, allowing for accurate simulation of molecular structures.

The style "real" was utilized during MD simulations as the standard units. Therefore, the following units were used in the MD simulations:

m (mass): gr/mole; r (distance): Angstrom; t (time): femtosecond; energy (Kcal/mole); velocity: (Angstrom/femtosecond); force: (Kcal/mole-Angstrom); temperature: (Kelvin); pressure: (atmosphere).